DOI: 10.1021/cg9013043

CRYSTAL GROWTH & DESIGN
Communication
2010, Vol. 10
1460–1463

Epitaxial Growth of *m*-Plane ZnO Thin Films on (10$\bar{1}$0) Sapphire Substrate by Atomic Layer Deposition with Interrupted Flow

Ching-Shun Ku,[†] Hsin-Yi Lee,*[,†,‡] Jheng-Ming Huang,[§] and Chih-Ming Lin*[,§]

[†]*National Synchrotron Radiation Research Center, 101 Hsin-Ann Road, Hsinchu Science Park, Hsinchu 30076, Taiwan,* [‡]*Department of Materials Science and Engineering, National Chiao Tung University, Hsinchu 300, Taiwan, and* [§]*Department of Applied Science, National Hsinchu University of Education, Hsinchu 300, Taiwan*

Received October 20, 2009; Revised Manuscript Received February 10, 2010

ABSTRACT: Nonpolar ZnO films were grown epitaxially on (10$\bar{1}$0) sapphire substrates at 200 °C by atomic layer deposition with interrupted flow. The latter method improved the crystalline quality of ZnO films, transformed the structure from polycrystalline to epitaxial, and enhanced the optical properties of near-band-edge emission. The interfacial structure shows multiple domain phases along sapphire (020) and the disappearance of a minor phase near the surface. As determined by X-ray diffraction, the epitaxial relation between ZnO and sapphire follows $[002]_{ZnO}\|[020]_{sapphire}$ and $[020]_{ZnO}\|[006]_{sapphire}$. The photoluminescence intensity increased with increasing crystalline quality and thickness of ZnO films.

Zinc oxide and its compounds are promising materials for broad optoelectronic applications, especially for solid-state devices that emit in the blue or ultraviolet (UV) regions or that emit white light, with advantages over III-nitride semiconductors such as a large exciton binding energy.[1−6] Orientation parallel to the *c*-axis is the preferred direction of growth of ZnO on most currently available substrates, but this orientation causes a spontaneous piezoelectric field within the active layers of a light-emitting device based on ZnO, resulting in a small luminous efficiency.[7,8] To improve the luminescence characteristics, nonpolar ZnO is preferable.[9,10] Atomic-layer deposition (ALD) is a self-limiting process to grow thin films that possess several practical advantages including accurate and simple control of the thickness, a large area and a large batch capability, effective conformality and reproducibility, straightforward doping and scaling, and the ability to produce sharp and tailored interfaces and to prepare multilayer structures; the latter property is required in a continuous process to fabricate optoelectronic devices.[11] Moreover, ALD generally yields a thin film with a polycrystalline structure on various substrates; a ZnO-based optoelectronic device with high performance requires preparation of epitaxial ZnO thin films of great quality. Some authors have reported demonstrations that an epitaxial thin film of the *c*-plane ZnO can be grown with ALD on a sapphire substrate and a buffer layer of GaN or yttria-stabilized zirconia (YSZ) grown with another method,[12,13] but there is no report of epitaxial growth of *m*-plane ZnO on sapphire by ALD without a buffer layer. Such epitaxial growth of ZnO on sapphire is of great importance for the fabrication of optoelectronic devices. We grew a *c*-plane epitaxial film of ZnO on sapphire using ALD with an interrupted flow.[14] Here we present the first report of epitaxial growth of a *m*-plane nonpolar thin film of ZnO on a (10$\bar{1}$0) sapphire substrate by ALD with an interrupted flow.

ZnO thin films were grown on a sapphire (10$\bar{1}$0) substrate using ALD; diethylzinc (DEZn) and water served as precursors for zinc and oxidant, respectively. The temperature of growth of the thin films was maintained at 200 °C. In conventional ALD, durations of pulses of DEZn and water precursors were 100 ms, respectively. After a precursor pulse was injected into the reaction chamber, highly pure N_2 gas was used to purge the chamber for 10 s at 1 Torr chamber pressure and evacuated with a rotary pump (6 s to 1 mTorr) before the next precursor was admitted to the chamber. For the interrupted flow, after evacuation of the chamber, the ALD valve was closed first to preserve the pressure of the precursor and to increase the duration of reaction between the precursor and the sample surface. The period of closure of the ALD valve, called the "stock time", was 3 s; the durations of pulses of DEZn and water were 30 and 60 ms respectively. Purging and pumping were performed in the same manner as with the conventional method. Thin films of ZnO were deposited with 100, 400, and 1600 ALD cycles to achieve thicknesses ~22.5, 100, and 400 nm, respectively.

Measurements of X-ray diffraction at high resolution (HRXRD) and of X-ray reflectivity (XRR) were performed at wiggler beamline BL-17B1 with an eight-circle diffractrometer in the National Synchrotron Radiation Research Center (NSRRC), Hsinchu, Taiwan. For XRD, the photon energy was 8 keV with a flux estimated to be 10^{11} photons/s. Use of two pairs of slits between the sample and the detector provided a typical wave-vector resolution ~0.001 nm^{-1} in the vertical scattering plane in this experiment. The image and nanobeam diffraction (NBD) patterns of high resolution transmission electron microscopy (HRTEM) were performed along the *c*-axis of sapphire substrate. Micro-Raman scattering was recorded (Jobin-Yvon U1000 double grating monochromator, resolution 0.4 cm^{-1}) with an Ar^+ laser providing excitation at 488 nm. For measurements of photoluminescence (PL) at 10 K, a He−Cd laser (325 nm, IK3252R-E, Kimmon) provided excitation with a UV-enhanced CCD (spec-10, Princeton Instruments, cooled with liquid nitrogen) after a monochromator (0.5 m, SP-2558A, Acton, entrance slit width 10 μm, grating 1200 L/mm, spectral resolution 0.02 nm).

Figure 1 shows XRD patterns measured from a radial scan ($\theta-2\theta$ scan) along the surface normal of ZnO films (400 ALD cycles, on a sapphire (10$\bar{1}$0) substrate) with and without interrupted flow. Values of *H*, *K*, and *L* given in this paper for an orthorhombic crystal system are expressed in reciprocal lattice units (r. l. u.) referred to parameters of the ZnO lattice, $a = 0.5628$, $b = 0.325$, $c = 0.5207$ nm at 25 °C. Thin films of ZnO deposited with continuous flow show a (200)

*Author to whom correspondence should be addressed. E-mail: hylee@nsrrc.org.tw (H.Y.L.); cmlin@mail.nhcue.edu.tw (C.M.L.).

 Published on Web 03/22/2010

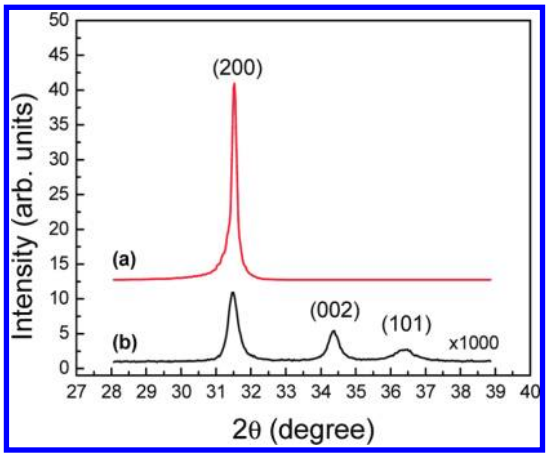

Figure 1. Surface normal of crystal-truncation-rod (CTR) scan spectra of a ZnO film (400 cycles) (a) with interrupted flow, and (b) without interrupted flow.

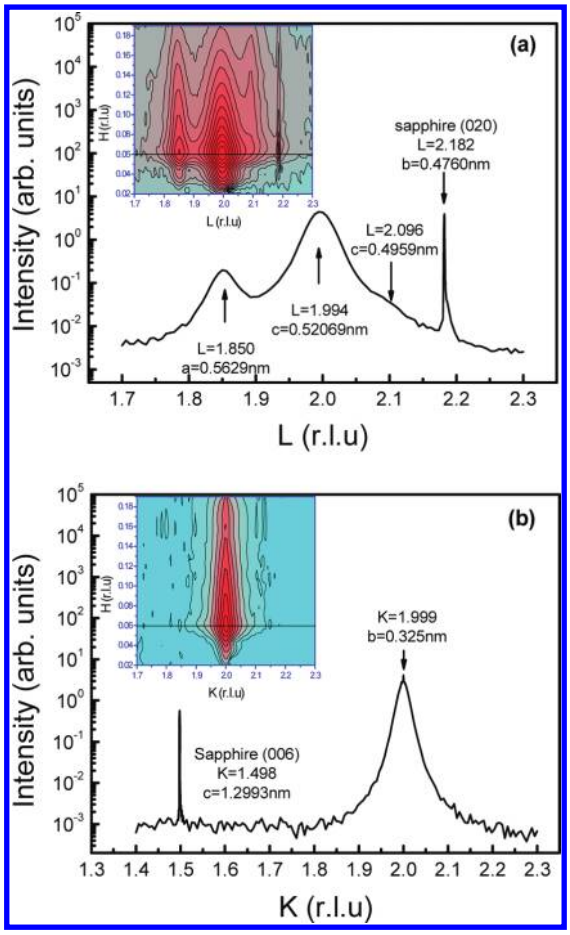

Figure 2. CTR spectrum (a) along the ZnO direction (0.06 0 *L*); the inset shows the dependence of the CTR scan profile on depth; (b) a scan along the ZnO direction (0.06 *K* 0); the inset shows the dependence of the CTR scan profile on depth.

preferential polycrystalline orientation, whereas a ZnO film grown with interrupted flow shows in the upper curve in Figure 1 only a single intense (200) feature. Moreover, the intensity of the (200) feature of ZnO with interrupted flow was 3000 times that of the conventional method. To examine the behavior of induced strain relaxation due to lattice mismatch at interfaces between ZnO and sapphire and the relation

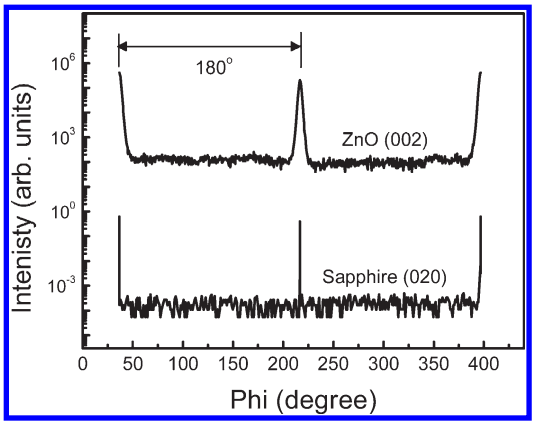

Figure 3. Azimuthal scan (Φ scan) of the surface ZnO (002) line and the substrate sapphire (020) Bragg line of a ZnO film deposited with 100 cycles.

between surface and orientation of ZnO and its substrate, we measured a map of the in-plane dependence of the crystal-truncation-rod (CTR) on the depth of thin (100 cycles) and thick (1600 cycles) films of ZnO. Figure 2a shows a *L*-scan of a thin film of ZnO (100 cycles). The scan was performed near the ZnO (002) Bragg line; the angle of incidence was fixed at $H = 0.06$ with respect to the sample surface during the measurement. The intense and sharp feature centered at $L = 2.182$ is the sapphire (020) Bragg reflection from the substrate, as shown in Figure 2a. Besides the sapphire (020) Bragg reflection, the feature at $L = 1.994$ is ascribed to unstrained ZnO (002). Two additional minor phases of ZnO appeared at $L = 1.850$ and 2.096, which might indicate a *c*-plane orientation (200) ($a = 0.5629$ nm) and partially strained ZnO (002) ($c = 0.4959$ nm), respectively. The existence of these minor phases might be attributed to release of strain due to a large lattice mismatch (~9.38%) between sapphire (020) and ZnO (002). The inset of Figure 2(a) shows in an *L*-scan the dependence of the CTR mapping on depth. The profile shows the *c*-orientation and that the partially strained phase became increasingly dominant for a position near the interface (for $H > 0.1$) or subordinate near the surface (for $H < 0.06$). Figure 2b shows a *K*-scan in a direction perpendicular to that of the *L*-scan with the same angle of incidence ($H = 0.06$); a broad feature at $K = 1.999$, indicated by arrows in Figure 2b, is ascribed to the Bragg line of ZnO (020), and a sharp Bragg line originates from the substrate (006) at $K = 1.498$. The lattice parameter of sapphire (006), ~1.2993 nm, is almost four times that of ZnO (020), 0.325 nm. In addition, a narrow feature on top of the ZnO (020) line indicated that ZnO was well aligned with sapphire through nearly a lattice match at the interface. The inset shows also that no other minor phase exists from the interface to the surface. Furthermore, an azimuthal scan near a ZnO (002) surface line and the substrate (020) Bragg line of a ZnO film deposited after 100 cycles, as shown in Figure 3, clearly exhibits a 2-fold symmetry with the same orientation. No other feature was observed in the intervals between the two lines, indicating a perfect alignment of $\vec{c}$ and $\vec{b}$ axes of ZnO unit cells along those of the sapphire substrate. These results provide firm evidence that a strongly epitaxial layer was deposited on the substrate. The CTR scan of Figure 2 and the azimuthal scan of Figure 3 indicate that an epitaxial relation between ZnO and sapphire follows $[002]_{ZnO} \| [020]_{sapphire}$ and $[020]_{ZnO} \| [006]_{sapphire}$.

To acquire insight into the detailed phase distribution of the structure, we examined CTR mapping along both *L*- and *K*-directions of the deposited ZnO films. Figure 4 shows the CTR mapping for ZnO films of 100 cycles and

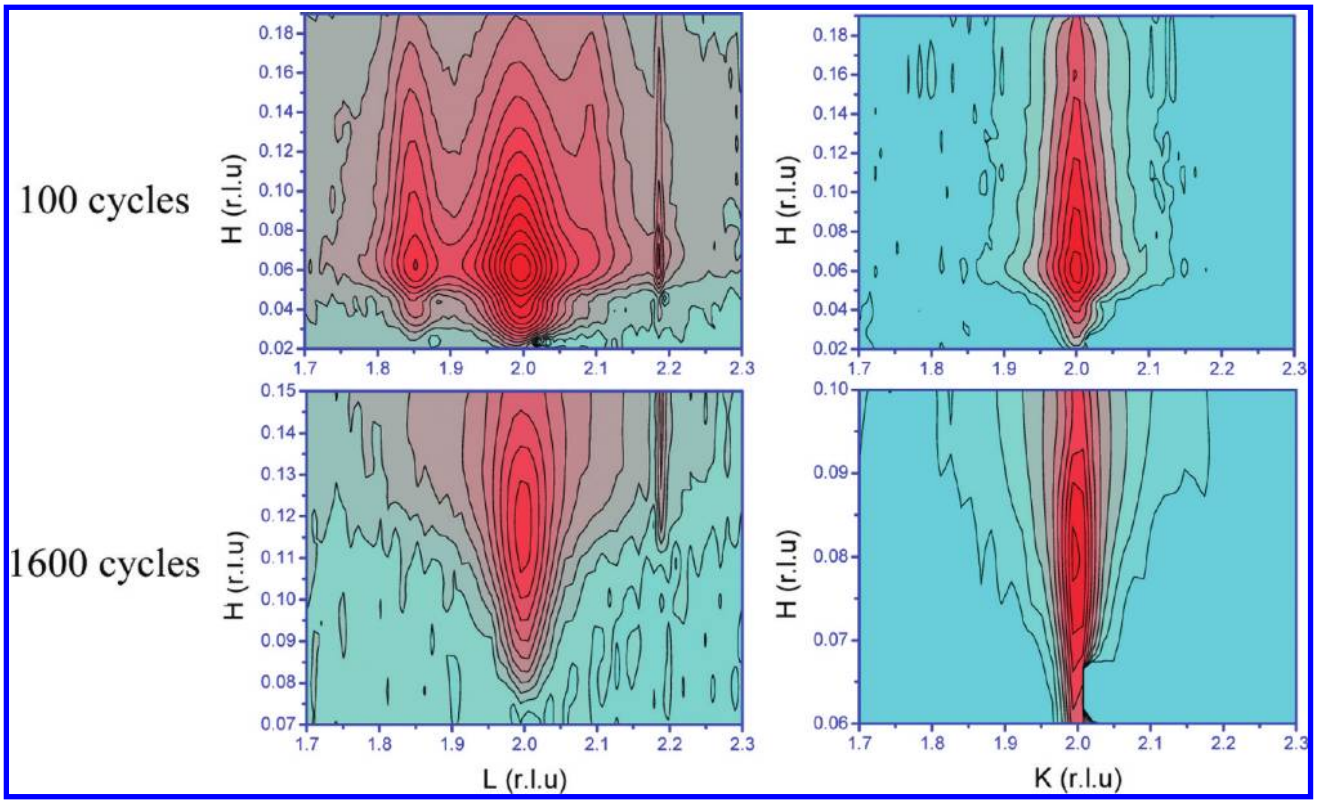

Figure 4. CTR maps of thin films of ZnO with 100 and 1600 cycles for each *L*- and *K*-direction.

1600 cycles, which were similar between thin (100 cycles) and thick (1600 cycles) ZnO films for *K*-direction mapping. In the *L*-direction, the thick ZnO film displays only a single phase of the ZnO (002) Bragg line. The intensity distribution was broad at large *H* but became narrow with decreasing *H*. The results clearly demonstrate that the minor phase completely vanished and the crystalline quality was improved with increasing thickness of the ZnO film.

To confirm the growth conditions and orientation relation obtained from HRXRD, we examined the HRTEM images and NBD patterns of the ZnO films. Figure 5a,b shows HRTEM images and NBD patterns for a ZnO thin film from 400 ALD cycles with continuous flow and from 1600 ALD cycles with interrupted flow, respectively. The HRTEM image in Figure 5a shows three grain boundaries and four distinct orientations along the *c*-direction of sapphire. From a comparison of NBD patterns between the interface, surface, and substrate, the diffraction spots also indicated a polycrystalline structure of the ZnO thin film with continuous flow. After 1600 cycles of growth of a ZnO thick film in the stock mode, the HRTEM image and NBD patterns showed a monocrystalline nature, with the lattice parameter ~0.521 nm in-plane along the (0002) direction. The large-scale TEM image shows that the dislocation density gradually decreased from the interface to the surface, in agreement with CTR maps compared in Figure 4.

Figure 6 shows the polarity dependence in the micro-Raman results. In this case, with *X*, *Y*, and *Z* constituting the Cartesian coordinate system, the *X* direction is perpendicular to the *m*-plane and *Z* is along the *c*-axis. When the polarization direction of the incident light is perpendicular to the *z* direction, we see two signals of the E_2^{high} modes of ZnO at 438 cm^{-1}, whereas when the polarization direction of the incident light is parallel to the *z* (polarization) direction, the E_2 mode is undetectable.[15] This experimental result demonstrates that the obtained sample is a nonpolar ZnO film with the *c*-axis lying in the growth plane, in accordance with the XRD results.

Figure 7 shows photoluminescence measured for ZnO films of varied thickness at 10 K; for comparison, a ZnO film (400 cycles) prepared with continuous flow is included in Figure 7. The film with interrupted flow shows much greater intensity in the donor-bound exciton (D_0X, 3.364 eV) and its related phonon replica emission (D_0X-1LO, 3.303 eV) region than with continuous flow, but both have similar intensity in the green band (GB). Furthermore, the 1600-cycle ZnO thin film showed a much clearer phonon replica with respect to other films, signifying a greater crystalline quality. The PL results show that, with increasing film thickness, both the emissions of ZnO related to D_0X increased rapidly and the GB emission due to oxygen and zinc vacancies is suppressed, indicating the quality of the thin film to have improved greatly, in agreement with TEM results. The cause of the PL behavior for a thin film was that the interface region contained several phases of ZnO; the grain boundary and boundary surface between phases produced many dislocations and vacancies that resulted in deep levels and contributed to GB emission.[16−18] When the film became thicker with only one domain phase, the GB emission decreased and donated the carriers to the near-band-edge (NBE) emission.

In conclusion, we used interrupted flow to grow ZnO as a thin film with *m*-plane orientation on $(10\bar{1}0)$ sapphire substrates. Interrupting the flow not only converted the growth structure from polycrystalline to monocrystalline but also promoted the quality of the thin film. Compared with our previous results on *c*-axis orientation,[14] both orientations show epitaxial growth via precursors with the interrupted method, but *m*-plane ZnO thin films possess superior crystalline quality and optical properties. An in-plane scan along the *L*-direction of ZnO was more complicated than that along the *K*-direction because of a larger mismatch of lattices between the thin film and the substrate. Minor phases existing in the *L*-direction vanished with increasing thickness of the film, and the ZnO (002) orientation also became narrowed through full relaxation of strain. Both the

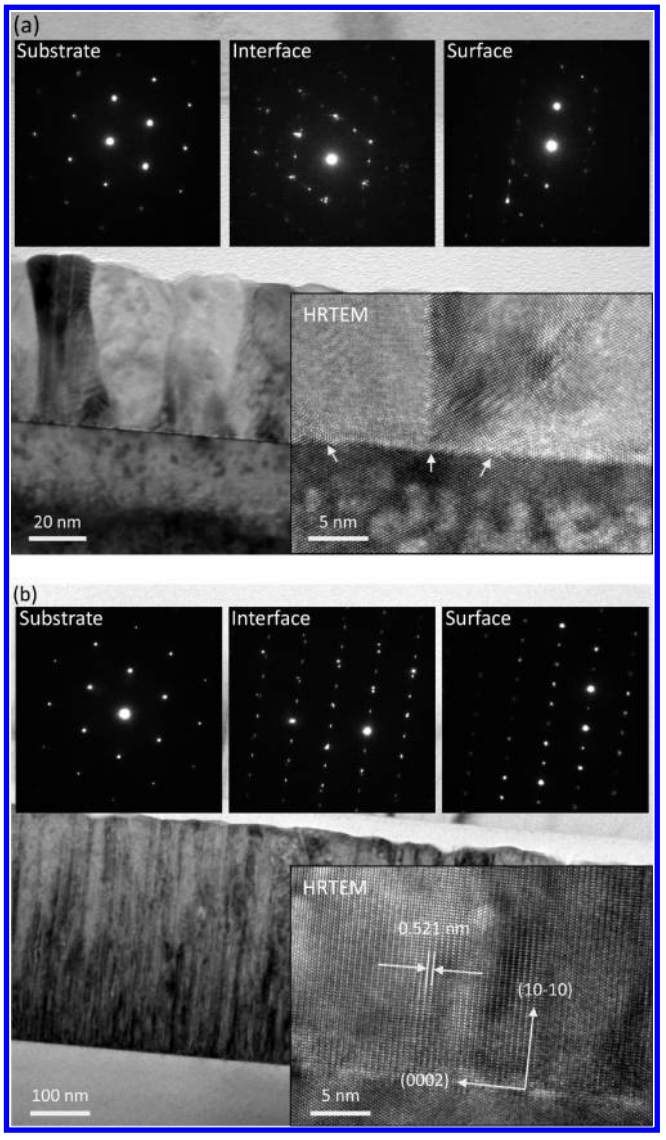

Figure 5. HRTEM images and NBD patterns of ZnO thin films: (a) 400 cycles without interrupted flow and (b) 1600 cycles with interrupted flow.

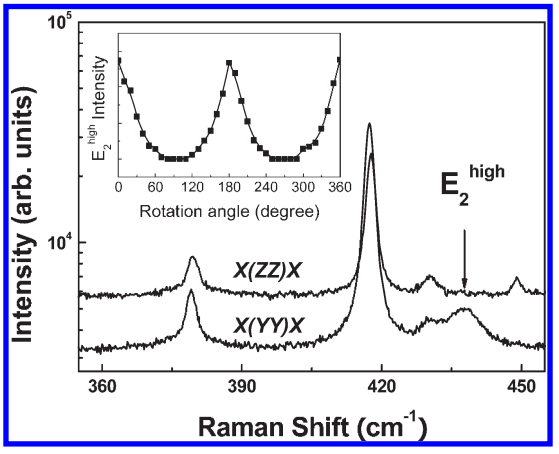

Figure 6. Micro-Raman scattering spectra measured at two scattering geometries; the inset shows the rotation intensity of the ZnO E_2^{high} peak.

photoluminescence intensity and the NBE/GB ratio increased with increasing crystalline quality and thickness of ZnO films.

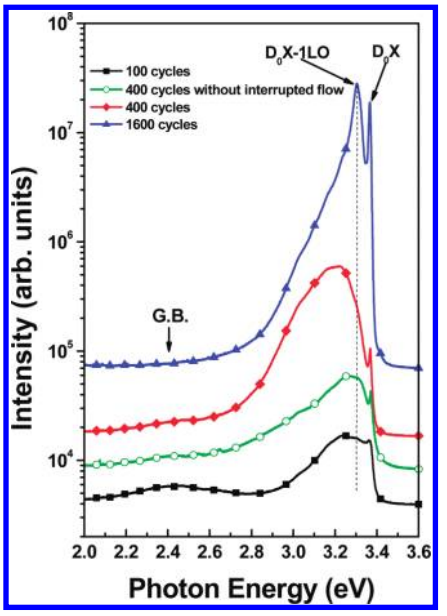

Figure 7. Photoluminescence of ZnO films at 10 K deposited with a varied number of ALD cycles.

Acknowledgment. National Science Council of the Republic of China, Taiwan, provided support under contracts NSC 98-2221-E-213-002 and NSC 97-2120-M-001-007.

References

(1) Tsukazaki, A.; Ohtomo, A.; Onuma, T.; Ohtani, M.; Makino, T.; Sumiya, M.; Ohtani, K.; Chichibu, S. F.; Fuke, S.; Segawa, Y.; Ohno, H.; Koinuma, H.; Kawasaki, M. *Nat. Mater.* **2004**, *4*, 42–46.
(2) Hofstetter, D.; Theron, R.; Shaer, A. H. E.; Bakin, A.; Waag, A. *Appl. Phys. Lett.* **2008**, *93*, 101109.
(3) Ryu, Y. R.; Lubguban, J. A.; Lee, T. S.; White, H. W.; Jeong, T. S.; Youn, C. J.; Kim, B. J. *Appl. Phys. Lett.* **2007**, *90*, 131115.
(4) Guo, Z.; Zhao, D.; Liu, Y.; Shen, D.; Zhang, J.; Li, B. *Appl. Phys. Lett.* **2008**, *93*, 163501.
(5) Sun, X. W.; Zhao, J. L.; Tan, S. T.; Tan, L. H.; Tung, C. H.; Lo, G. Q.; Kwong, D. L.; Zhang, Y. W.; Li, X. M.; Teo, K. L. *Appl. Phys. Lett.* **2008**, *92*, 111113.
(6) Newton, M. C.; Shaikhaidarov, R. *Appl. Phys. Lett.* **2009**, *94*, 153112.
(7) Waltereit, P.; Brandt, O.; Trampert, A.; Grahn, H. T.; Menniger, J.; Ramsteiner, M.; Reiche, M.; Ploog, K. H. *Nature* **2000**, *406*, 865–868.
(8) Im, J. S.; Kollmer, H.; Off, J.; Sohmer, A.; Scholz, F.; Hangleiter, A. *Phys. Rev. B* **1998**, *57*, R9435.
(9) Tian, J. S.; Liang, M. H.; Ho, Y. T.; Liu, Y. A.; Chang, L. *J. Cryst. Growth* **2008**, *310*, 777–782.
(10) Ho, Y. T.; Wang, W. L.; Peng, C. Y.; Liang, M. H.; Tian, J. S.; Lin, C. W.; Chang, L. *Appl. Phys. Lett.* **2008**, *93*, 121911.
(11) Niinisto, L.; Ritala, M.; Leskela, M. *Mater. Sci. Eng., B, Solid-State Mater. Adv. Technol. 196*, 41, 23−29.
(12) Lin, C. W.; Ke, D. J.; Chao, Y. C.; Chang, L.; Liang, M. H.; Ho, Y. T. *J. Cryst. Growth* **2007**, *298*, 472–476.
(13) Satio, K.; Nagayama, K.; Hosokai, Y.; Ishida, K.; Takahashi, K. *Phys. Status Solidi C* **2004**, *1*, 969–972.
(14) Ku, C. S.; Huang, J. M.; Lin, C. M.; Lee, H. Y. *Thin Solid Films* **2009**, *518*, 1373–1376.
(15) Cuscó, R.; Alarcón-Lladó, E.; Ibáñez, J.; Artús, L.; Jiménez, J.; Wang, B.; Callahan, M. J. *Phys. Rev. B* **2007**, *75*, 165202.
(16) Vanheusden, K.; Warren, W. L.; Seager, C. H.; Tallant, D. R.; Voigt, J. A.; Gnade, B. E. *J. Appl. Phys.* **1996**, *79*, 7983–7990.
(17) Wu, X. L.; Siu, G. G.; Fu, C. L.; Ong, H. C. *Appl. Phys. Lett.* **2001**, *78*, 2285.
(18) Reynolds, D. C.; Look, D. C.; Jogai, B.; Van Nostrand, J. E.; Jones, R.; Jenny, J. *Solid State Commun.* **1998**, *106*, 701–704.